PROJECT DESCRIPTION

Studies of Cosmic Ray Muon Radiation and its Application to Archaeometry

Mark Adams, Edmundo Garcia-Solis[b], Joseph Sagerer[c], Eduardo Perez de Heredia[d]

[a] Physics Department, University of Illinois at Chicago
[b] Department of Chemistry, Physics and Engineering Studies, Chicago State University
[c] Department of Physical Sciences, Dominican University
[d] Frecuencia Cero Technology for Conservation

1. Introduction

This proposal requests support for a project of research and education in archaeometry and experimental physics. The project consists of the construction of detector hardware, associated electronics, and the data analysis tools necessary for developing a muon tracker to measure cosmic ray radiation and to use it for detecting substructures (that include cavities, such as tombs) inside Mesoamerican pyramids. This project will involve students at Chicago State University (CSU), a Predominantly Black Institution; and Dominican University (DU), a Hispanic Serving Institution, thus enabling the training of students traditionally underrepresented in STEM disciplines.

In recent decades, significant advances have been attained in our knowledge of the Mesoamerican culture. Many disciplines have contributed to this effort, including traditional archeological studies but also anthropological, ethnological, environmental, osteological, linguistic, mathematical and sociological studies, to name a few. Not only has archaeology has been enriched by all these disciplines, but archaeometry studies have finally become commonplace. Archaeometry is the application of scientific techniques to the analysis of archaeological samples, and a series of new purpose-specific methods and techniques are constantly developed for this field.

In this document, we propose an archaeometry tool for the detection of sub-structures inside Mesoamerican monumental constructions. The prehispanic monumental architecture was often achieved by the constant growth of the main buildings, which rose in height and expand as the centuries went by, leaving a sequence of buildings and contexts in stratigraphic order. Also, some Mesoamerican constructions were erected atop significant topographical features, such as caves and waterholes. Mesoamerican cultures usually took painful efforts to guarantee the preservation of the buildings of their ancestors, as they covered them with their own, and since they are protected by later constructions appear in better conditions of preservation. Customarily, the exploration of these sub-structures has been made physically, leading to a series of problems of conservation. In this regard, remote sensing techniques are extremely valuable both for the research and for the conservation of these ancient remains.

Specifically, we plan to take advantage of the absorption of cosmic ray muons in limestone, the material of which these buildings were constructed. This technique is not new: it was employed successfully for the first time in Egypt in 1969 by Nobel Laureate Luis Alvarez at the Second Pyramid of Giza [1]. The equipment used by Alvarez was bulky (it occupied a volume of 80 m^3) and delicate (the detector was primarily a collection of "spark" chambers). Since that time, technological advances have made the technique much more practical, and in 2017, a European collaboration deployed several muon detectors in the Khufu's pyramid finding the location of several cavities [2].

As we explain below, we will be able to construct a small, durable, reusable apparatus at a modest cost, able to withstand the extreme environmental conditions of sub-tropical weather, and that can be deployed over a period of time at different monumental sites. To this end, the technology and the size of the apparatus are crucial to the project. The techniques developed in this project and the experience obtained will allow

for the construction of improved future detectors at less cost and designed for specific applications. Dissemination of this information will allow other groups to develop their detectors.

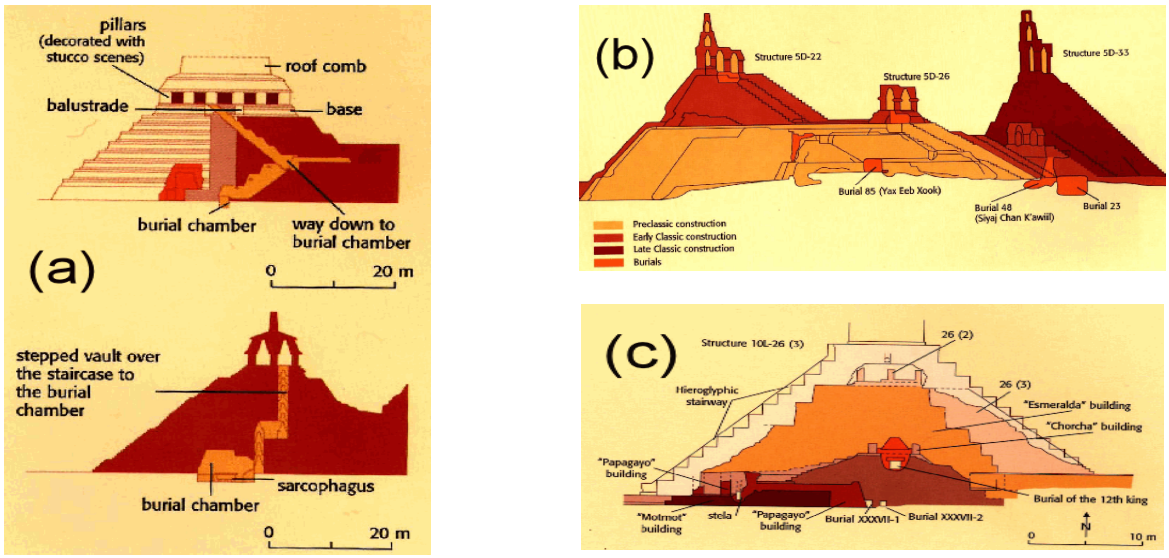

Figure 1: Locations of sub-structures at some of the major Mesoamerican sites [7]. (a) Palenque, where the sub-structure is at ground level. (b) Tikal, where several sub-structures are above ground level. (c) Copan, where the location of a sub-structure is above ground level.

Many of the best preserved architectural art have been found in sub-structures. Significant finds in recent years include discoveries in the Pyramid of the Moon at Teotihuacan (1999), at Copan [3] (1997), at Calakmul [4] (1999) and Tikal (1999) using traditional exploring techniques. The method we propose herein is to carry out substructure detection without disturbing the structure that surrounds them. The knowledge generated by these proposed investigations will be of great utility in the planning and execution of future explorations and conservation works.

Archaeometry has been applied in Mesoamerican sites using a range of methods. For example, a pioneering Ground Penetrating Radar (GPR) survey was conducted in 1993 by L. Desmond near the east facade of the Castillo Pyramid at Chichen Itza, Quintana Roo, revealing some cavities near the northeast corner [5]. In 1999 a sub-structure was discovered in temple XX at Palenque using non-intrusive ground penetrating radar [6]. Computer advances have made this technique a practical way of determining cavities. However, GPR has a severe drawback: if the cavities are small, they can only be detected a few meters below the surface. Longer wavelength electromagnetic waves have to be used to penetrate to greater depths, and this causes a loss in resolution rendering the method impractical for detecting small chambers deep inside the buildings.

Muons with a wide range of energies survive to the Earth's surface, and those that have energies larger than 15 GeV [11] can penetrate about 30 m of limestone; it is these muons that we wish to employ. The easiest way of understanding the principle of the method we wish to use is to imagine bullets being fired from many guns at a big pile of sand that has an empty cavity inside it (Fig. 2 left). If all the bullets were traveling at high enough velocity, they would all emerge on the other side of the sand. However, if some of the bullets are not moving so fast, a few will be stopped by the sand. The bullets stopped after having traversed the cavity will be less than the number that had to traverse sand throughout. This example illustrates the basic principle of the method we propose to use, using cosmic ray muons instead of "bullets."

We have carried out extensive simulations using the simulation application GEANT4 [12] which calculates all the physical processes that muons undergo (with the correct probabilities) when they traverse any

material, in our case, limestone. Some of the results are displayed in Fig. 3(a) where we show that there is a significant difference in the flux of 15 GeV muons that emerge from traversing 30 m of solid limestone compared to those that have traveled through 25 m of limestone and 5 m of the air-filled cavity. This difference decreases for higher energy muons (Fig. 3 (b) and Fig. 3(c)) because a more significant fraction of them has enough energy to survive 30 m of limestone. If the flux of muons arriving at the Earth's surface were independent of the muon's energy the technique that we are proposing here would not be valid. However, the muon energy spectrum is strongly dependent on energy with the flux decreasing by approximately a factor of 2 for every 5 GeV increase in energy (Fig. 2, right). So, as the probability of a muon of penetrating limestone (cavity or not) increases (due to its higher energy) its flux decreases.

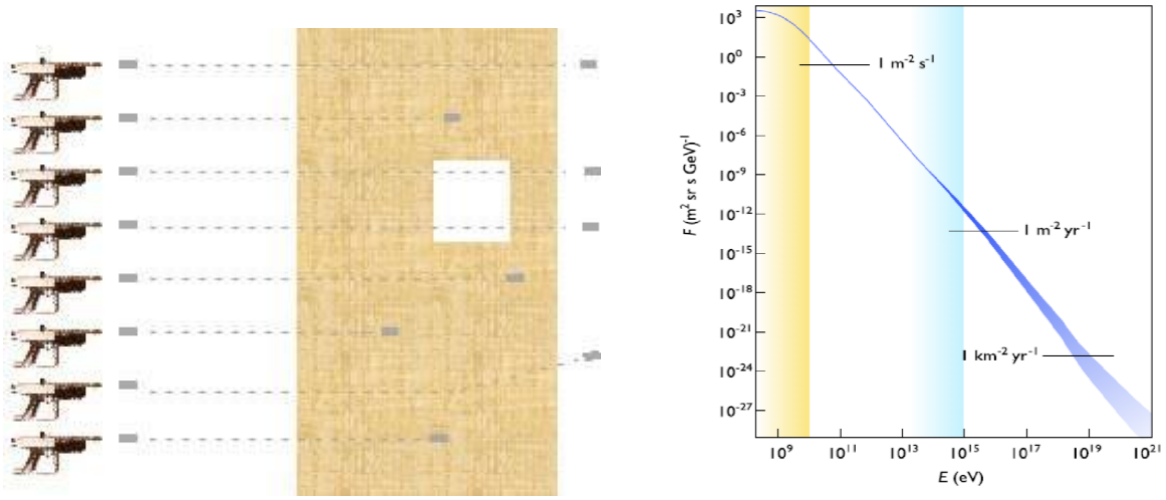

Figure 2. (Left) Illustration for the principle of using cosmic rays for detection of cavities. (Right) The energy spectrum of cosmic rays [10].

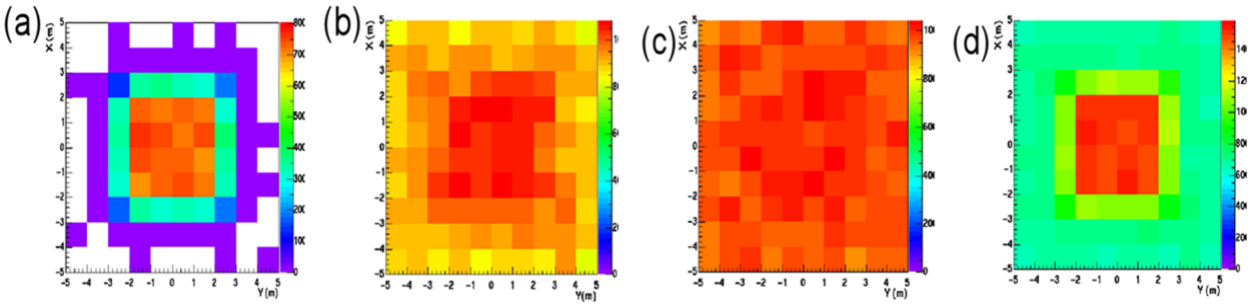

Figure 3: Proof of principle behind the proposed experiment. These four false-color pictures show the intensity of muons that survive traversing a limestone structure 30 m thick and a 10 m by 10 m cross-section area. The structure had a cube of side length 5 m placed centrally inside it. Red color denotes many muons; blue denotes few, white denotes none. We simulated muons to be vertically incident on the top face of the limestone, and we allowed them to have different energies: (a) 15 GeV, (b) 20 GeV and (c) 25 GeV. We can see from (a) that only muons that have traversed the cavity survive to the bottom of the limestone structure. The effect of the cavity is still apparent with 20 GeV muons. Finally, the effect becomes undetectable when 25 GeV muons are studied. The accumulative effect, with the correct energy dependence of the muon spectrum, included, as shown in (d). The presence of the cavity is clearly apparent.

2. Results from previous NSF Support

Over the last seven years the High Energy Experimental Nuclear group at CSU has been supported by NSF with the most recent grants: "Studies of Relativistic Heavy Ions Collisions in ALICE at the LHC," PHY-1613118 8/01/2016 - 8/02/2019, and MRI Consortium: Development of the Fast Interaction Trigger Detector for the ALICE Experiment at the LHC," PHY-1625081, 07/28/2016 - 07/29/2020. Recent ALICE

publications resulting from these grants are listed in references [30-45], and recent presentations given by faculty and students are listed in references [46-54].

Our research group has taken on shared responsibilities and duties that have contributed to the success of the ALICE experiment, including experiment-monitoring shifts, data analysis, detector maintenance, calibrations, paper, and talk reviews, etc. We have been involved in the design, simulation, and prototype testing of the Fast Interacting Trigger (FIT) [13]. We have studied the performance of the recently installed di-jet calorimeter (DCal) in simulations, and we are involved in two physics analysis topics. Our group proposed the study of the topology of the jets associated with the J/ψ decay, as a means to understand the production mechanisms of the J/ψ prompt and jet quenching in Pb-Pb collisions. Also, we began an investigation of the production of strange particles in jets.

CSU has been very fortunate in that twenty-two of its students have had the opportunity to work with ALICE at the Large Hadron Collider (LHC) at CERN. All found the experience to be rewarding. The project described in this proposal is synergetic with the ALICE program, as it combines particle physics, the building of instrumentation, and archaeology; the proposed research will undoubtedly attract new students to our physics and engineering program, motivating them to the pursuit of careers in the STEM. Furthermore, this collaborative research will be mostly based at our Universities, so it will be easier to link it to our outreach and recruiting activities, as described below in the Broader Impact section.

3. Research Program

The proposed tracker is designed for use in muographic imaging of the interiors of large, massive structures. The main application for the detector that we propose is the scanning the interiors of Mesoamerican constructions through the measurement of the muon flux. Atmospheric muons generated by cosmic rays can be of extremely high energy, many of these muons pass unimpeded through vast masses like volcanoes, others, the most energetic can penetrate several kilometers into the Earth [14]. Muography makes use of this passage of muons through the material to form images similar to how radiography makes use of the passage of x-rays through the material.

The detector is placed adjacent to or within an interior space near the bottom of the subject structure to produce a muographic image, the rate of muons hitting the detector is measured at various angles over several hours or days. Each angle measurement (zenith and azimuth) represents a path of muons through the subject structure (track). By knowing the external dimensions of the structure, one can compute the expected path-length for each track. The detector is then moved to view the open-sky and the measurement of rates at each angle is repeated. Using known energy-loss rates per path-length in the structure material and calculations of the muon energy spectrum at the structure's location the open-sky data is simulated to match the imaging data for a solid structure. Any angles in the imaging data with an excess of muons detected compared to the solid-structure simulation correspond to paths with less material than expected. The excess indicates the presence of a hidden void in the material. The presence of many adjacent voids indicates a hidden chamber within the structure, as represented in Fig. 4.

The proof of principle experiment for this use of muons to image large structures was done in 1955 [13] by measuring the thickness of rock above a mine (the overburden) using vertical muon rates. As mentioned in the introduction, in 1970 a team led by Luis Alvarez used the technique to search the second pyramid of Cephren in Egypt for chambers, his group was able to detect the four corners of the structure successfully but did not find any hidden voids [1]. Menchaca made similar unpublished efforts in the sun pyramid of Tenochtitlan [15], and more recently an experiment using muon detectors in the Khufu's pyramid found the location of several cavities [2]. When used for archaeometry, the tracker that we propose has several advantages. It is multi-directional, simultaneously measuring rates at many angles. It has a large enough active area to have high rates of detected muons. It has a sufficient number of channels, and each is sized to give angular enough resolution to image hidden chambers of greater than $1m^3$ in a limestone structure of

50 m thick. It is compact and easily movable allowing the structure to be entirely scanned from multiple angles and allowing it to be moved to other structures quickly.

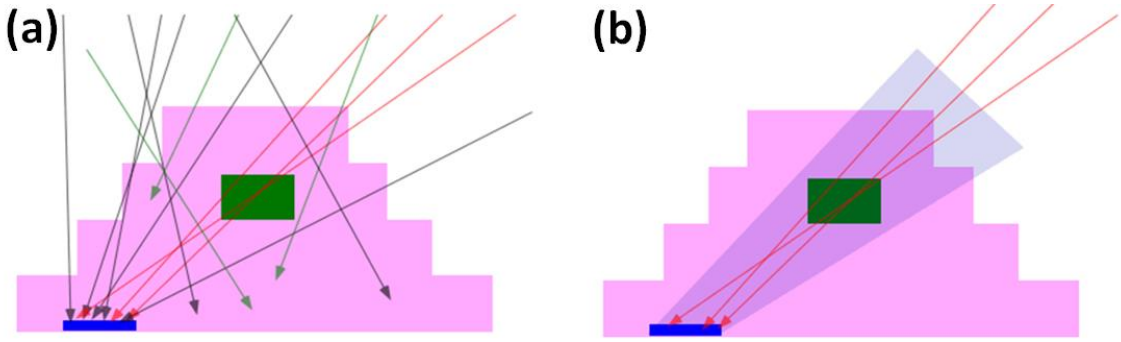

Figure 4. The diagrams represent the function of the tracker. (a) Trajectories of muons traversing the apparatus regardless of their direction. (b) Trajectories of muons that are required to be detected in the apparatus and to have trajectories within a defined angular range that corresponds to a chamber.

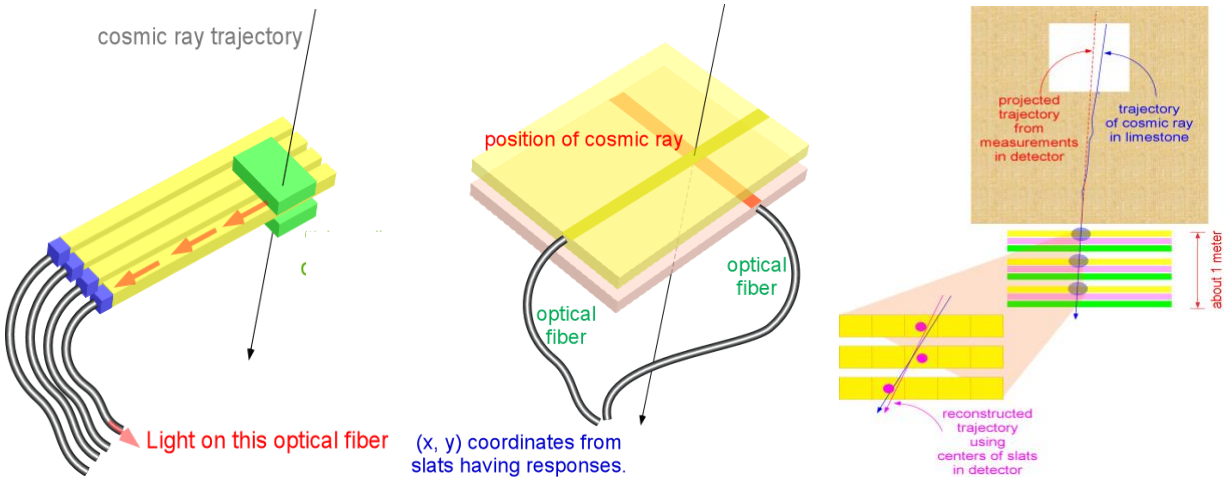

Figure 5. (Left) Principle of the apparatus, a muon goes through a scintillator slat producing light that is carried out by an optical fiber. (Center) The principle of reconstructing a location of a muon in a plane using two planes of slats arranged orthogonally to produce an X-Y grid. (Right) Several planes of scintillators will unambiguously define the trajectory of each muon traversing the tracker. We show here the effect of extrapolating a trajectory from a muon that has scattered in the limestone. We also show, in the magnified insert, the effect of the width of each slat on reconstructing a trajectory.

The use of atmospheric muons for imaging has other applications. In geology, the same technique described above has been used to determine the density of material within a volcano's magma chamber [16]. The only difference is that in this application, one assumes the material varies in density but contains no voids. Due to the need to place a detector far from the volcano to image it in its entirety and the significant loss of muons in such a large structure, the images produced in this application are similar to traditional two-dimensional radiographs. In national security applications, the scattering of muons by high-Z material (material with atoms of large atomic number) is used to scan cargo non-destructively. In this application, muon's paths are tracked by large detector arrays on both sides of the cargo. Rather than looking for a loss of muons due to large path-lengths, these detectors track the paths of muons before and after passing through the cargo. If high-energy muons are deflected by a large angle, it indicates the presence of a high-Z material. Due to their need for fast imaging and two-track reconstruction, these detectors have very large detection areas and are fixed in place. Since they reconstruct muon paths from multiple directions, they perform three-dimensional muon-tomography.

3.1 The Tracker Detector

To detect the presence of a muon, we will use material consisting of scintillating plastic. This material produces small amounts of light when an electrically charged subatomic particle travels through it (for our application these particles are the muons). The light moves through the transparent scintillator and is transported to a photosensitive device via an optical fiber. The light emerging from the fiber has to be converted to amplified electrical pulses. The light amplification can be done using several different techniques. We propose to use silicon photomultiplers (SiPMs). The resulting electrical pulse can be digitized and stored in electronic equipment and then read into a computer for analysis. To reconstruct the trajectory of the muons, we need to two points of their path, to this end; we propose to build a detector capable of detecting the position of the point (X, Y) of entry of the muon in the scintilla tors for at least two planes. The principle of how the detector works is illustrated in Fig. 5.

Much of the design described below is based on the experience gained in simulations and building and studying the performance of the prototype detector. The prototype served a testbed for the full detector elements, readout and data acquisition system. It also served as a test setup to develop data analysis software. The simulations helped to estimate the performance of the detector in field conditions. In section 3.2 we describe the simulation studies, and in section 3.3 we review and describe the prototype detector and the studies performed with it.

3.1.1 Active Hodoscope

The detector layout consists of a hodoscope (segmented detector that detects charged particles and determines their trajectories) comprised of 400 1m-long, 1cm-by-1cm slats of extruded plastic scintillator [17]. The slats are arranged into four planes of 100 sticks each. The four planes are separated into two grids made up of two adjacent planes with the slats in orthogonal orientations. Each grid is 1m^2 with 100 *X*-slats and 100 *Y*-slats (see Fig. 5), this gives a segmentation of 10,000-1cm^2 active areas per grid. By knowing the *X* and *Y* slats struck by a muon passing through them, the *X*-*Y* location of the muon intersection in each grid is known to within ± 0.5 cm.

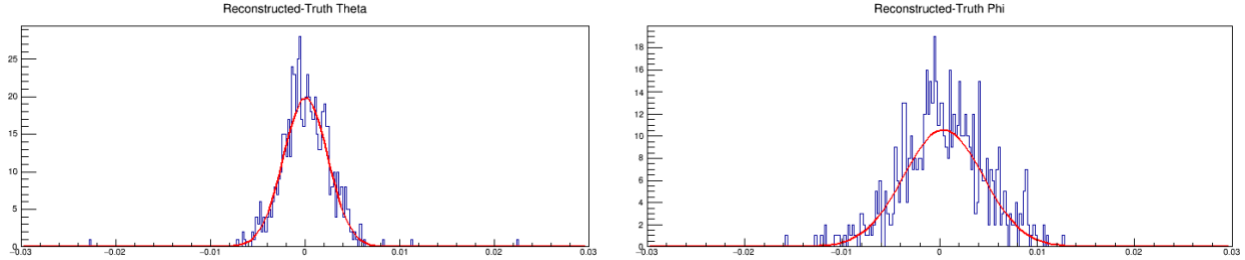

Figure 6. Difference between reconstructed track angles and true track angles in radians for zenith (left) and azimuthal (right) directions.

In the nominal geometry, 1m separates the two grids, Grid A and Grid B. When a muon goes through the detector, we will know two points (x_A, y_A, z + 1m) and (x_B, y_B, z) that can then be used to reconstruct the trajectory of the muon track). The dimensions of the detector give an azimuthally dependent maximum zenith angle acceptance of 45° (azimuthal angles 0°, 90°, 180°, and 270°) to 54.7° (azimuthal angles 45°, 135°, 225°, and 315°) with respect to the normal direction to the grids. Based on active area size and grid geometry, the intrinsic zenith angular resolution is angle dependent varying from ±0.81° for normal direction tracks to ±0.14° for maximum angle tracks. The intrinsic azimuthal resolution is angle dependent as well ranging up to ±0.41º for maximum zenith tracks. In detector simulations with track reconstruction, the standard deviation for the difference in reconstructed direction vs. true-direction was 0.13° for zenith angle and 0.23° for the azimuthal angle, as shown in Fig 6.

Based on simulations of muons moving in a pyramid, and hitting the tracker inside a chamber after penetrating 20m, we find that the average scattering angle between the initial muon direction and the

direction of the muon hitting the top of the detector peaks around 1.5°±0.8° (mean ± sigma) for muons with an initial momentum of around 15 GeV/c. We also find that the average energy loss by the muons is 0.5 GeV per meter. The scattering angle is the primary source of uncertainty in the measurement of the direction of the muons, driving the experimental resolution of the tracker. The experimental resolution is larger than the intrinsic resolution of the detector. So, in principle, the 1x1 cm^2 cross-section of the scintillators could be increased. However, in doing so, we would lose resolution if we use the detector for other applications where the multiple scattering is not so significant. We would also lose the flexibility to change if needed, the configuration of the detector; for example, by reducing the distance between the grids, as explained below. Furthermore, with the current design, we could decrease the effect of the multiple scattering by hardening the muon spectra, by adding a Fe slat between the grids.

The nominal spacing between the grids allows a geometrical acceptance of 35% of all azimuthal and zenith angles for the hemisphere above the detector representing an area of 2.2 sr. Based on the known open-sky flux of 1 muon per cm^2 per minute in the surface of the earth [18], it is expected that each grid will be exposed to muons at a rate of 167 Hz. However, the geometrical acceptance of the detector lowers this to 58 Hz for unobstructed measurements. Changing the separation between the grids can change the geometrical acceptance, but any change in the *z* spacing of the grids also affects the angular resolution. Moving the grids apart lowers the geometrical acceptance and event rate, but improves the angular resolution of each possible pair of grid locations. Moving the grids closer increases geometrical acceptance and rate, but at a loss of angular resolution. Should the imaging of an archeological site yield exciting results, the grid separation could be reconfigured to adjust the detector's resolution and get a sharper signal of a cavity.

In addition to the geometrical acceptance of the tracker, there are gaps between the slats of the grids and some muons will cross through the edges of the scintillators that further reduce the detection rate. For the simulations, a tracking algorithm was implemented to merge adjacent hits due to muons passing through two adjacent slats, around half of the events had a muon passing through an edge in at least one of the four planes. The issue is for the muons that go through an edge of a slat without going into an adjacent slat, leaving a signal that is below the hit threshold, so that the edges of the slats create inefficiencies in the track reconstruction. The gaps between the slats are small; there is a coating on the scintillators that allow them to be placed adjacent to one another. The coating thickness varies, but it is an approximately a quarter of a millimeter. The gaps reduce the acceptance by 5% per slat. Combining the geometrical acceptance, the tracking reconstruction inefficiency and the gap acceptance effects, from simulation studies, we calculate that the total efficiency of the tracked is of around 20%. Reducing this number by 5% due to the two-hit events that produce tracking ambiguity, we end up with a total 19% efficiency of the detector. Another effect to consider is the two or more muon hits since these events generate ambiguous tracking solutions for the orthogonal grids, and they will be discarded. We have measured the 2-muon open-sky rate arranging 25 by 30 cm scintillator detectors in a $1m^2$ area. We found that the 2-muon hit rate is of about 5% of the total hit rate expected in each grid for our application. The rate for triple more muon events is not significant.

In order to discern $1m^3$ chambers installing the detector 10 m below the cavities, we need to sample the hemisphere above the detector in 2° cones, there are about 200 of such cones in the detector acceptance, so that in order to obtain a 1% statistical error measurement we would require 10,000 counts per cone or 2 million events. The full-open sky rate is 168 Hz, but the total efficiency of the detector is of 19% so that the open-sky event rate of the tracker is of around 32 Hz, from simulations we estimated that this rate is reduced by a factor of 20 underneath a pyramid, so that the effective event rate is of about 1.5 Hz. Thus we expect compliting a 1% measurement run (2 million events) in 370 hrs. or 15 days.

The details of the cost of the detector are in the Budget Justification sections of the proposal; it is of approximately $400.00 per channel, that includes the total cost of the equipment, materials, and supplies, and a 10% contingency per channel.

3.1.2 Light Sensing and Readout

Each of the 400 scintillator slats has embedded in it a 1.01m long, 2mm diameter BDF92 wavelength shifting fiber manufactured by Saint-Gobain [19], 0.01m of the fiber extends beyond the scintillator and acts as a light guide for signals to be routed to Silicon photomultipliers (SiPMs). Each slat and fiber will be coupled to a 2 x 2 mm active area Hamamatsu S13360-2050VE SiPM [20]. The SiPMs are mounted on carrier boards that sit in bores which permit them to be pushed up against the fibers. A counter motherboard with spring-loaded pins makes electrical contact with the SiPM carrier boards. Signals from the counter motherboards are sent to the front-end board by HDMI cables. The signal is then amplified and digitized in the front-end boards as explained in the following section. The original carrier board system was designed by Fermi lab and the University of Virginia for the Mu2e experiment [21], we plan to use a modified version of this board for our detector.

3.1.3 Trigger and Data Acquisition System (DAQ)

The DAQ hardware makes use of hardware designed for the Mu2e cosmic-veto. It consists of seven 64-channel Mu2e digitizer boards [22] to analyze signals and store event information, and one Mu2e controller board to make trigger decisions and synchronize readout of the data. The DAQ system receives 400 electronic signals from the SiPMs mounted in groups of 4 on mounting boards modified from the Mu2e design and arranged to match SiPM spacing used in this detector. Since the SiPM gain is temperature dependent, each mounting board also contains a temperature sensor. Each group of 4 signals is transmitted on one of one hundred HDMI cable to the digitizer board where a 12-bit ADC is used to convert signals to digital values. The same cables transmit voltage to the SiPMs and the temperature sensor data.

Firmware running in on-board field programmable gate arrays (FPGA) continuously buffer signal history and act as an adjustable discriminator for each signal. When one of the electronic signals exceeds the threshold set in the firmware discriminator, a logic signal is generated in the FPGA. The FPGA continuously monitors all channels for this logic signal and outputs a logic signal to the DAQ controller board when it detects that the plane has had an element struck. The DAQ controller board is used to communicate to the digitizing boards, to synchronize their clocks, and change their settings. It monitors the digitizing boards watching for a 4-way coincidence in digital signals indicating that all four planes of the detector were struck simultaneously. It then tells firmware on the digitizer board to analyze the history of each channel's ADC. Based on this the digitizer boards write for each channel the timing of any signals, integrated ADC, and an event timestamp. The files are then written to the external DAQ computer. The firmware and software run on the digitizing and controller boards will be modified from the Mu2e originals to match the logic required by the proposed detector.

3.1.4 Software for Data Collection, Detector Monitoring, and Analysis

Various pieces of software will be used for the proper operation of the detector system. A graphical user interface is used to set trigger conditions and thresholds in the DAQ and controls the readout of files from the DAQ digitizer boards. It can also allow readout of full ADC waveforms at a greatly reduced rate of operation during the testing/commissioning phase of operation. This control and monitoring software will be run on a single external DAQ computer. The DAQ computer will be connected wirelessly to the internet; this will allow the transference of raw data to our institutions. This is how we will monitor the gain of the SiMPs, the quality of the data and the performance of the detector. The data will be saved in duplicate at CSU and DU servers.

Geant4 [23] is used in the analysis to perform simulations of the passage of muons through the structure to be imaged and the detector. It is a stable, standard simulation toolkit used by many high-energy Physics experiments and has the capabilities required to created simulated data. The Root data analysis tool [24] designed and maintained by CERN will be used to take the raw data files from the DAQ and assemble them into combined events with information from all digitizer boards. It also reads the simulated data from

Geant4. Once this initial combining is performed, the Root code will be further used to analyze the data to produce images.

3.1.5 Mechanical Structures

The detector will be mounted in a sturdy, yet lightweight aluminum frame. Grid A and Grid B will each be mounted along with the fibers, SiPMs and carrier boards in light-reducing enclosures lined with rigid closed-cell foam to further reduce outside light. Each enclosure is then mounted to a cubic frame 1m on a side. The frame is attached to a base that can be tilted to several angles. A separate rugged 19-inch rack contains the DAQ boards and DAQ computer.

3.2 Simulations

The detector's ability to image structures was tested via simulation of the detector's response to atmospheric muons using the Geant4 [23] software package. The detector's active elements were constructed in software in an air-filled volume along with a target pyramid made up of a flat-topped, four-sided pyramid out of Calcium Carbonate (the primary component of limestone). The pyramid's dimensions approximate the temple of El Castillo at Chichen Itza [25, 26]. Positive muons were fired in the downward direction towards the detector. The response of the detector was first tested in the absence of any pyramid (open-sky). Simulations were performed for the detector in a void in the structure directly below a 2 m^3 void, and for the detector placed externally adjacent to the pyramid but tilted 60° from vertical such that the pyramid filled the acceptance of the detector, to demonstrate the versatility of the detector (Fig. 7).

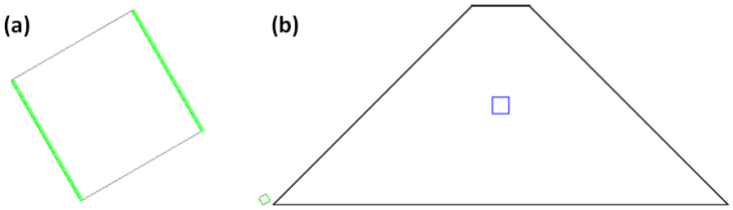

Figure 7. Detector geometry for the detector adjacent to the pyramid: (a) The detector elements, tilted in the direction of the pyramid, (b) the detector adjacent to the pyramid containing a 2m^3 air-filled chamber.

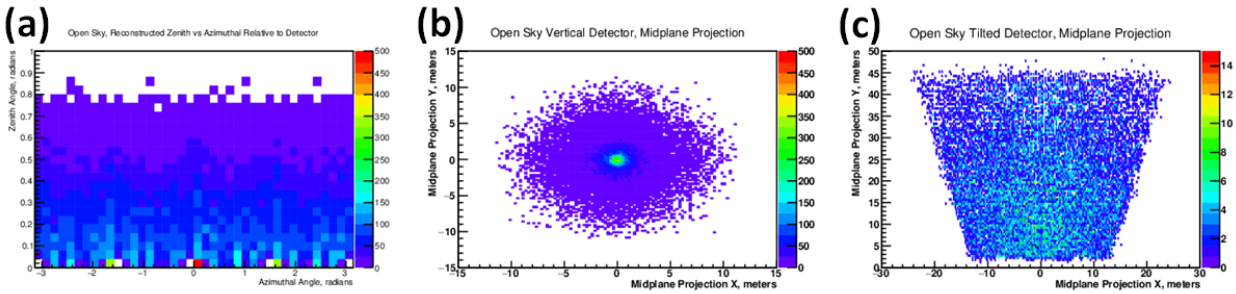

Figure 8. "Open-sky" detector simulations. (a) Zenith angle versus azimuthal angle both in radians for reconstructed tracks, angles are relative to normal to detector face, (b) projection of tracks to horizontal plane at midpoint of pyramid for vertical detector looking up through Pyramid, (c) projection of tracks to vertical plane at midpoint of pyramid for detector tilted 60° from vertical looking sideways through Pyramid. Projection units are in meters.

For the detector placed below the chamber, the direction of the muons was randomly chosen in azimuthal angle and randomly chosen according to the nominal $\cos^2\theta$ distribution in azimuthal angle for muons at sea level. For the detector placed adjacent to the pyramid, the simulations were limited to only the 180° of an azimuthal range containing the pyramid. For the tilted detector, the zenith direction has been corrected for

angular distribution for image clarity. No additional corrections have been applied; other corrections for detector acceptance and expected path length in the material can be used to clarify the images further.

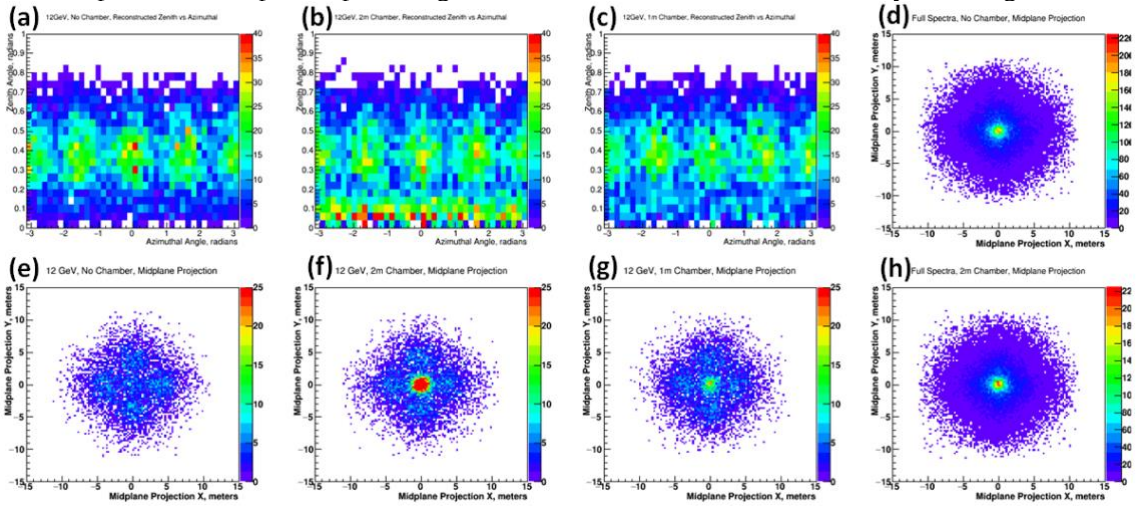

Figure 9. Reconstructed simulation results for vertically-directed detector: Zenith vs. azimuthal angle, both in radians for (a) 12 GeV no chamber, (b) 12 GeV 2 m^3 chamber, (c) 12 GeV 1 m^3 chamber. The four regions of excess hits in azimuthal angle are due to the relatively shorter path length through the faces of the pyramid. The chamber is visible in (b) and (c) near zero azimuthal angles along the bottom of the graph. Projections to a horizontal plane midline to the pyramid's height are shown for (e) 12 GeV no chamber, (f) 12 GeV 2 m^3 chamber, (g) 12 GeV 1 m^3 chamber. The faces of the pyramid show along the two axes. The chambers can be seen in the excess tracks at (0 m, 0 m) in (f) and (g). Projections based on the full muon energy spectrum are shown for (d) no chamber and (h) a 2 m^3 chamber. The chamber can be seen as an excess of tracks (approximately 9% for the center bins) at (0 m, 0 m) in (h).

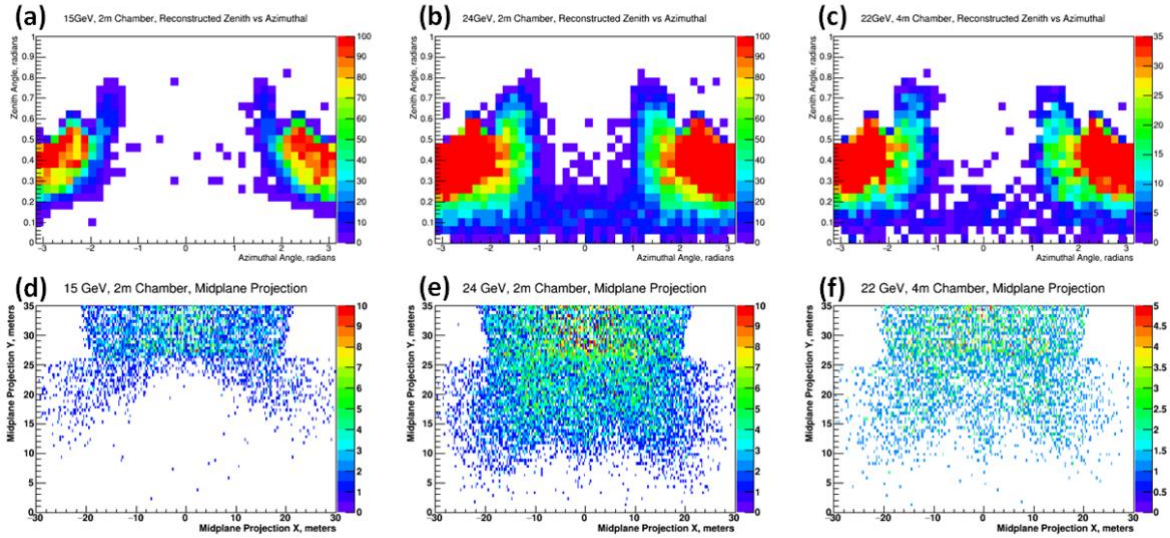

Figure 10. Reconstructed simulation results for director tilted 60° from vertical: Zenith vs. azimuth angle relative to the detector normal, both in radians for (a) 15 GeV 2 m^3 chamber, (b) 24 GeV 2 m^3 chamber, (c) 22 GeV 4 m^3 chamber. Projections to a vertical plane midline to the pyramid's width are shown in (d) 15 GeV 2 m^3 chamber, (e) 24 GeV 2 m^3 chamber, (f) 22 GeV 4 m^3 chamber. In (a) and (d) the muons' energies are too low to pass through the pyramid showing a shadow devoid of tracks. The outline of the pyramid can clearly be seen in (d). Particles secondary to collisions produce the fringe tracks at wide angles. In (b) and (e) the energy is now sufficient for some tracks to pass through the thinner top of the pyramid as well as the section of the chamber. In (c) and (f) a larger chamber shows clearly without corrections.

For each simulated run, one hundred thousand muons were fired towards the detector at fixed energies from 10 GeV to 25 GeV in 1 GeV steps or a distribution randomly distributed to match the energy at the chosen θ following the parameterization of [27]. In each, reconstructions of tracks were performed from hits in each of the two grid planes. Additional to raw angular distributions, projections to planes located at the midpoint of the pyramid were performed. For the vertical facing detector, the projection is to a horizontal plane at half the height of the pyramid above the ground this simulates the view upwards through the pyramid. For the tilted detector, the projection is to a vertical plane bisecting the pyramid parallel to the face of the detector this simulates the view sideways through the pyramid. To see detector acceptance, Fig. 8 shows each detector scenarios for no pyramid (open-sky). Select energies for each simulation scenario with the pyramid are shown in Figs. 9 and 10.

3.3 Detector Prototype

The design of the tracker and choice of materials is based on the project team's experience with detector systems in high-energy physics experiments. In addition to this knowledge, a prototype 16-channel (four 4-channel planes) was assembled and tested at CSU and DU, using seed funding. In all elements, the design considers capability, dependability, robustness for field deployment, and cost. The prototype has four 4-scintillator stick planes forming two 4-by-4 grids with single channel photomultiplier tubes (PMT).

There are several ways to track the paths of charged particles. The original Alvarez experiment in 1972 used spark chambers, which require sealed gas chambers requiring maintenance and bulky gas subsystems. Since then there have been many detector advances. Among them, GEMs and silicon-based systems have a very high spatial resolution, but both require cooling, and are sensitive to shock. Drift tubes such as those deployed in port security applications need large subsystems and have an unpractical (for the applications of this project) large detector size. These facts leave scintillator detectors with readout by light sensors as the proven detector technology. The main advantage of these detectors is the robustness. The scintillators are hard plastic or crystal, they are easy to assemble, the materials are easy to mill and shape to mount to the frame structure, and sturdiness to environmental effects.

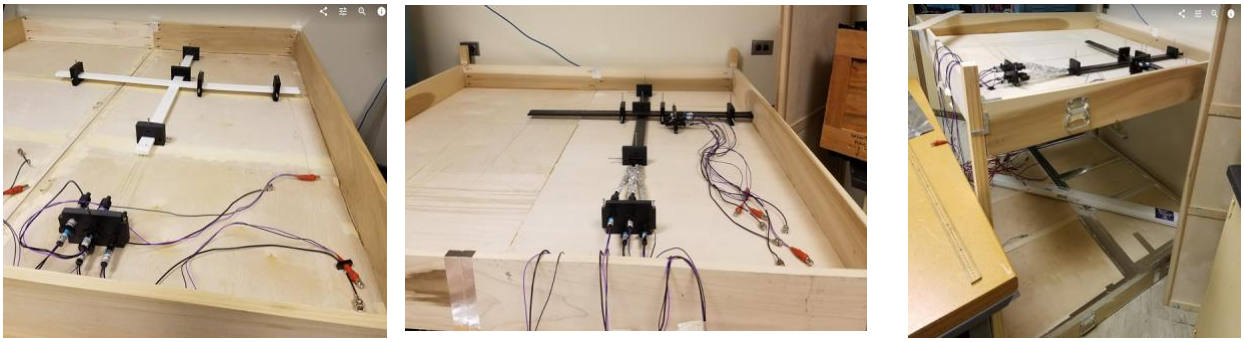

Figure 11. Prototype setup: left-one of the 4-by-4 grids before full assembly, a middle-upper grid with elements wrapped in light-tight coverings, right-the two boxes separated by 1 meter containing the grids. The top cover has been removed from the upper box showing the upper grid.

Cost primarily drives the determination of the scintillators type. Crystal scintillators have a high-energy resolution but are not readily available in the long, thin elements that are needed for a grid hodoscope. On the other hand, plastic scintillators, are available in long pieces with numerous combinations of cross-sections. They are manufactured using two processes: casting and extrusion. Cast scintillator is heated until it flows and in cast into molds under low pressure to extract bubbles. The manufacturing process is both labor and time intensive making cast scintillator costly but of high optical quality. It is optically clear and allows long light paths before absorption, often longer than the length of the element itself. This fact means that light produced at one end of the element will travel to the far end of the element where it can be read out. We ran preliminary 1-meter-long single-element tests on cast scintillator varying from thin 2 mm

diameter fibers to 1cm by 2 cm square slats. Typical costs were on the order of $100 per element excluding any waveguides or fibers. All scintillators that we tested were able to produce light signals detectable by PMTs. The light then is needed to be moved from the ends of the detector elements to the multichannel PMTs. This implied two possible additions, either a light guide added to the end of the element would transfer the light to a clear fiber optic cable, or a wavelength shifting fiber would be embedded in the scintillator element. The best light signals were achieved by embedding and optically gluing a wavelength shifting fiber into a milled groove the length of the 1 cm by 2 cm slat.

In testing the single channel element, the cast scintillator with an embedded wavelength shifting fiber inserted (but not glued) had a loss in efficiency of 10% less than the embedded and glued wavelength shifting fiber in the cast scintillator. This loss was acceptable as a tradeoff for cost savings. We acquired a total of 16 1m long extruded scintillator elements and tested them in two configurations using single channel PMTs for readout. In the first setup, four parallel scintillators were placed side-by-side in a light-tight box. We tested the flexibility of the wavelength shifting fibers, by embedding 2 mm diameter fibers in the scintillators. The 1.2 m fibers were bent to an angle of 45° at a distance of 5 cm, and the 1.5 m fibers were bent 180° at a distance of 16 cm. The signals from th PMTs were then discriminated, and coincidences between all four channels were tracked for several weeks. Once it was determined that the detector elements would be a hodoscope made of extruded scintillator with embedded glued WLS fibers, the method of converting the light signals to electrical signals was addressed. In single element testing, available Hamamatsu H5211 hybrid photomultiplier tube assemblies were used. Hamamatsu R647 single channel PMTs were used in the multichannel testing and prototype due to the available of low cost used tubes. For each setup, a Wiener MPOD crate with Ethernet control and a 16-channel High Voltage card was used to power the PMTs. This setup had several issues for the scalability to a 400-channel full detector.

If one were to use 400 single channel PMTs, this would necessitate 25 high voltage (HV) cards and a total of 5 MPOD crates to hold them along with 400 HV cables. Also, mounting 400 PMTs would require an additional frame structure. This compelled to test silicon photomultipliers (SiPMs) for our application. The SiPMs thet we used have an area of 2 x 2 mm and can be mounted directly to the scintillator slats, and the power for the SiPMs (they use less than 40V of regulated voltage instead of HV) can be directly fed on the readout motherboards through a standard HDMI cable. The SiPMs have the advantage of lower cost per channel than the PMTs. We tested the SiPMs with the scintillator-fiber slats. Using a stack of three scintillator-fiber-SiPM units we tested for the efficiency of the SiMPs by measuring the number of events when the muon produced a signal above threshold in the first and third units and comparing it with the number of similar events found in the middle unit, we find that the units have an excellent efficiency of 99.97%. We also tested the gain of the SiPMs and found it compatible for the hodoscope. Finally, we measured the signal from the muons crossing the scintillator around 97 cm away from the SiPM at the other end of the slat, and 2 cm away from the SiPM. We found a difference in the amplitude of the signals of less than 10% at the operational gain of the SiPM.

It has been reported [28] that the gain for the Hamamatsu S13360-2050VE SiPM is dependent on the temperature (2% per 1°C), we do not expect significant variation of temperature over the run periods for our application, and we plan to monitor the gain of the tubes during the run in order to implement correction to possible significant changes in the gain of the sensors. We found that is equivalent to use SiPMs instead of multichannel PMTs four our application, and that the SiPMs have the advantage of being powered with low voltage, lower cost, and more important: that we can take advantage of existing readout, and data acquisition electronics for our application from a current high energy physics experiment: Mu2e.

The last requirement of the detector is to trigger event readout based on the electronic signals from the SiPMs then readout the channel information sufficient to reconstruct muon tracks. The first operation is to discriminate the signals based on pulse heights to determine that a channel was struck. Each struck channel generates a logic signal. After that, a logical OR of each plane is generated; a triggered event starts when

all four planes generate a logic signal from the OR of their 100 channels. Readout of which channels are struck then requires that each channel have information readout – integrated pulse, ADC. Once this information is available, the DAQ software assembles the channel information for the event and writes it to a computer file. Most large experiments with many channels of electronic signals to readout currently use boards operating on the VME standard. We had several concerns with this traditional approach. It necessitates several VME crates and many boards. This will add to the detector's footprint onsite and the complexity of the readout wiring and cost. We priced a VME system from CAEN that included (4) 128-channel discriminator boards, TDC boards, a board to perform the logical decisions, and the necessary crates with controller boards. The price was approximately $360 per channel excluding added cables needed. It included no advanced logical capabilities based on the individual signal sizes or location and included no ADC information.

Instead of off the shell standard VME electronics, we have settled on the use of Mu2e cosmic-veto digitizing boards and controller board with modified SiPM mounting boards and modified fiber guides. The digitizing boards contain four onboard FPGAs that are used to perform firmware discrimination and trigger logic; they also have on-board power for the SiPMs. The Mu2e experiment uses these boards to power and readout SiPMs connected to fibers form plastic scintillators in a different geometry from the proposed detector. These boards have been extensively tested to meet the extremely high-efficiency required by the Mu2e veto. By being part of the large order of boards, we can greatly reduce our readout costs. This brings the equipment and supply cost per channel for the DAQ to approximately half the cost of the VME system. It also includes three additional digitizing boards and one spare controller, the Mu2e cosmic-veto digitizing also eliminate the extensive cabling needed in the VME system. The Mu2e boards also allow for more advanced logic based on the relative timing of signals. They can provide integrated ADC information and can provide a complete ADC history (waveforms) for each channel at a reduced operating rate. Such information is extremely valuable for periodic detector testing and monitoring. By tracking ADC with time, the health of the SiPMs and the light generating elements can be monitored.

3.4 Construction Plan, Timeline, and Responsibilities

The construction plan for the full detector can be divided into two Phases. During Phase I, 64 channels of the detector system will be assembled and tested. Phase I has a timeline of approximately one year. Phase II will be final assembly and commissioning of the full 400 channel detector. Phase II has a timeframe of approximately two years. DU will be responsible for the readout electronics, data acquisition system, and the development of the data analysis tools, CSU for the construction and assembly of the detector, including the mechanical structures. Both Universities will work on the integration, commissioning and testing. Professor Mark Adams experience in the D0 detector is significant for the design of the readout system of the tracker that we propose. He will be also critical for the integration of this detector to the QuarkNet program as described in Section 4.

Phase I begins summer of 2019. The timeline along with the responsibilities of each institution is laid out in Table I. The Mu2e DAQ board, and control board has a long development and construction timeline. The final specifications for our unique board requirements will be completed in consultation with Mu2e in the summer of 2019. This gives sufficient time for procurement and the assembly of the parts needed for 64 channels of the detector, to be completed in the spring of 2020 when one readout card and one DAQ board will be available. The testing of a full 64 channel system, within the existing prototype enclosure, including the readout and DAQ will be done through the summer of 2020.

Phase II begins the Fall of 2020 with the acquisition of the rest of the boards for the readout and DAQ, and the assembly of the full 400 channels of the detector. By the summer of 2021, we will have the full detector built, together with all the readout and DaQ electronics. During the fall of 2021, and the spring of 2021 our groups will work on the mechanical structures and the development of the data analysis tools, to have the detector integrated, commissioned and tested by the end of the summer of 2022.

Table I. Phase I timeline.

PHASE I	Pre-Grant	Fa19	Sp20	Su2020
Readout and DAQ Development (DU)				
SiPM Mounting Board Modifications (DU)				
Materials and Acquisitions (DU, CSU)				
Prototype run of modified SiPM mounting boards and Modified Fiber guides (DU)				
64 channel detector assembly (CSU)				
Readout and DAQ testing (DU)				
64 channel Hodo, Readout and DAQ testing (CSU, DU)				

Table II. Phase II timeline.

PHASE II	F2020	S21	Sum21	Fa21	Sp22	Sum22
SiPM boards and fiber acquisition (DU)						
Assembly of full Hodo channels (CSU)						
Readout and DAQ testing (DU)						
Mechanical Structures drawings (CSU)						
Data analysis tools development (DU)						
Mechanical Structures construction (CSU)						
Integration and testing (CSU, DU)						

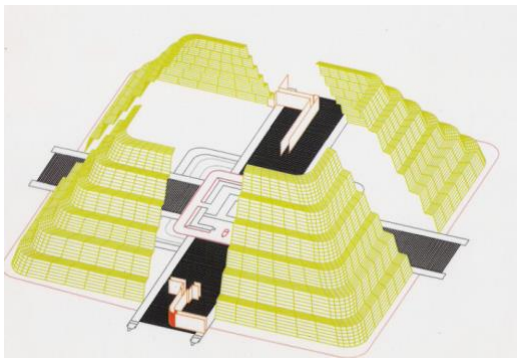

Figure 12. (Left) Picture of El Castillo pyramid at Chichen Itza. (Right) AutoCAD drawing of the pyramid, which shows the location of a tunnel at the base.

3.5 Construction, Testing and Deployment phase.

The authors of this proposal have the interest and technical expertise to carry out this project to its conclusion. After the construction and testing of the detector, we anticipate no problems in involving experts from different disciplines onto the project the next phase of the project: moving the detector to an archeological site and searching for cavities inside constructions. The authors of this proposal have already held informal discussions with officials of the Instituto Nacional de Antropologia e Historia (INAH) in Mexico. This government organization has identified sites where they believe that there is a good probability of sub-structures of major importance being located. The most accessible is in Chichen Itza. El Castillo pyramid is ideal for this application; the pyramid has a tunnel at the base with suitable dimensions for the detector and power outputs (Fig.12) a picture of the pyramid, and AutoCAD drawing showing tunnel at the base. Furthermore, there is a known chamber in its interior that can be used to commission and teste the detector, and then collecting data to search for hidden chambers. After the exploration of El Castillo pyramid, we would work with the Mexican archaeologist to explore other sites suitable for the technique that we propose: Uxmal, Yucatán, Pyramid El Adivino. Izamal, Yucatan, Pyramid Kinich Kakmo. Coba,

Quintana Roo, Pyramid Nohoch Mul. Edzna, Campeche, Pyramid of The Five Stores. Xochicalco, Morelos, Pyramid 1. Cacaxtla, Tlaxcala, Pyramid 1. Monte Alban, Oaxaca, South Pyramid. El Tajin, Veracruz, Pyramid of The Niches.

Dr. Perez de Heredia, senior personnel and co-author of this proposal, is a Mexican archaeologist with more than 30 years of experience in the Maya area, where he has conducted major excavations and architectural restorations at Kabah, Uxmal and Chichen Itza among others. After many years of working in different capacities for governmental institutions, his interest in sensing techniques prompted him to start a consultancy, Frecuencia Cero, specializing in technological applications for the conservation and research of the cultural heritage in Mexico. He will be critical in the exploration phase of the project.

4. Broader Impacts

The development of instrumentation for cross-disciplinary studies provides an attractive opportunity to both captivate and train students. Given the makeup of the student population of our institutions, this project has the potential to draw more underrepresented students into the STEM and train them in archaeometry, in detection instrumentation techniques, and in the development of code for data capturing and analysis. This collaborative proposal between CSU and DU will give our students the opportunity to participate in a captivating research program, engaging them in analysis and hardware projects in which they gain valuable skills and the opportunity to collaborate with experts from areas outside physics. These experiences will allow our students to transition successfully to their professional lives.

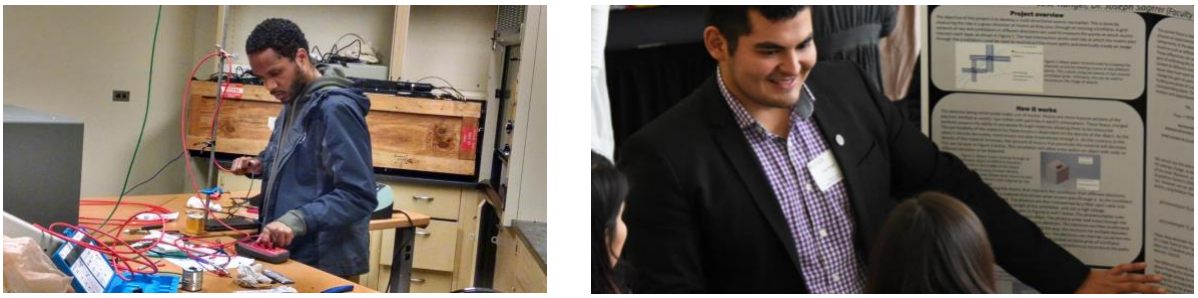

Figure 13. (Left) CSU physics student, working on the detector laboratory. (Right) DU student presenting his poster "Prototype Cosmic-Ray Muon Tracker" at an undergraduate research symposium.

The proposed project has the potential for an important link to the group's outreach activities. CSU is part of QuarkNet [29]. Through QuarkNet, our group extends its experiences with this research program to high schools in the area. Our current activities include workshops, directed research on cosmic ray experiments, and visits with high school students to UIC, CSU, Adler Planetarium and Fermilab. CSU is the link between Thornton South High School, Brooks High School, Noble Pullman College Prep, and QuarkNet. These inner-city high schools serve underrepresented minority students so that the combination of QuarkNet and this program constitutes a tool for recruitment of minority students into STEM disciplines. The QuarkNet network in Chicago is interested in the study of high-energy cosmic rays through the detection of "showers," several kilometers in radius. The showers consist of the highest-energy particles ever observed in nature and thus of current interest in the astrophysics and particle-physics community [30]. QuarkNet is led by Dr. Adams in the greater Chicago. In this region, the program has a network of detectors at different high schools that are used to study these shower events. Currently, the individual detectors used in the QuarkNet network are capable of measuring cosmic ray flow, but not the direction of the tracks. The direction has to be established with time correlations with other detectors in the area. This method is not efficient for calculating the low flux of extended air showers and results in a large uncertainty in the measurement of the direction of the showers. If we include in the detector network the tracker detectors we are proposing here, we will increase the probability of detecting high-energy events, and we will be able to improve the directional measurements.